RESEARCH ARTICLE

Check for updates

Photochromic spiro-indoline naphthoxazines and naphthopyrans in dye-sensitized solar cells†

José-María Andrés Castán, [ID] *[a] Valid Mwatati Mwalukuku,[a] Antonio J. Riquelme,[b] Johan Liotier, [ID][a] Quentin Huaulmé, [ID][a] Juan A. Anta,[b] Pascale Maldivi [ID][a] and Renaud Demadrille [ID] *[a]

Photochromic dyes possess unique properties that can be exploited in different domains, including optics, biomedicine and optoelectronics. Herein, we explore the potential of photochromic spiro-indoline naphthoxazine (SINO) and naphthopyran (NIPS) for application in photovoltaics. We designed and synthesized four new photosensitizers with a donor−pi−acceptor structure embedding SINO and NIPS units as photochromic cores. Their optical, photochromic and acidochromic properties were thoroughly studied to establish structure–properties relationships. Then, after unravelling the possible forms adopted depending on the stimuli, their photovoltaic properties were evaluated in DSSCs. Although the photochromic behavior is not always preserved, we elucidate the interplay between photo-chromic, acidochromic and photovoltaic properties and we demonstrate that these dyes can act as photosensitizers in DSSCs. We report a maximum power conversion efficiency of 2.7% with a NIPS-based dye, a tenfold improvement in comparison to previous works on similar class of compounds. This work opens new perspectives of developments for SINO and NIPS in optical and photovoltaic devices, and it provides novel research directions to design photochromic materials with improved characteristics.

1. Introduction

Photochromic compounds are a specific class of molecules that can undergo photo-induced transformations between isomers with different optical properties.[1] During the last decades, many families of organic molecules with photochromic properties have been identified and studied in detail.[2,3] Most of them involve monomolecular reaction mechanisms such as photocyclizations, isomerization reactions and intramolecular proton transfer to carry out their photoswitch. Among photochromic molecules, diphenyl-naphthopyrans,[4] spiro-indoline naphthopyrans,[5] spiro-indoline naphthooxazines,[6] diarylethenes[7] or azobenzenes[8] stand out. Due to their appealing properties, they can be employed in a wide variety of applications,[9] ranging from data storage,[10] actuators,[11] sensing[12] and ion detection,[13] optical lenses,[14] holographic recording devices[15,16] or bioimaging,[17,18] to name a few. Despite decades of research on photochromes, their use in photovoltaics is very recent.[19]

However, these compounds could be particularly interesting for the design of semi-transparent devices because their reversible transformation between the two forms with different absorption would allow obtaining solar cells whose transparency could be modulated according to the light intensity.[20] Such a property would be particularly appreciable in Building Integrated Photovoltaics (BIPV).[21,22] Nevertheless, very few photochromes have been tested in photovoltaic devices. In 2015, a bis-thienylethene derivative was first used in dye-sensitized solar cells (DSSCs).[23] For this type of molecules, the interconversion between the different photo-isomers is only possible by alternating ultraviolet and visible light irradiations. In addition, the colored isomer led to a poorer power conversion efficiency (PCE).

Photochromic dyes from the spirobenzopyran and spirobenzo and naphthoxazine families were also tested in DSSCs.[24] Here again the isomerization process required intense ultraviolet irradiation and the molecules did not lead to the reversible optical properties expected within the device. Besides the fact that they were not stable, their photovoltaic performances were extremely low with PCEs below 0.1%. The low performance of these molecules can be explained by an unsuitable molecular design for this application. Indeed, in most of these systems, the anchor function was not conjugated with the photochromic core, which resulted in poor charge injection into the photoelectrode.

[a] Univ. Grenoble Alpes, CEA, CNRS, IRIG-SyMMES, 38000 Grenoble, France.
E-mail: renaud.demadrille@cea.fr
[b] Department of Physical, Chemical and Natural Systems, Universidad Pablo de Olavide, Carretera de Utrera km 1, Sevilla 41013, Spain
† Electronic supplementary information (ESI) available. See DOI: https://doi.org/10.1039/d2qm00375a
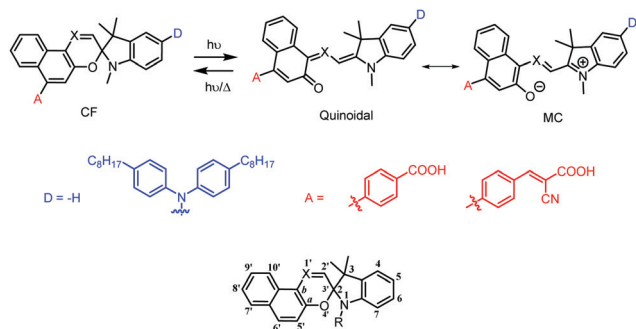
Scheme 1 General structure of the SINO (X = N) spiro[indoline-2,3′-[3*H*]naphth[2,1-*b*][l,4]oxazine and NIPS (X = CH) spiro[indoline-2,3′-[3*H*]naphtho[2,1-*b*]pyran derivatives synthesized in the present work as well as the interconversion reaction between their close (CF) and open quinoidal and merocyanine forms (MC).

We have recently demonstrated that naphthopyran-based derivatives, when properly designed, show a high potential in semitransparent DSSCs.[20] Push–pull photochromic naphthopyrans can sensitize efficiently TiO_2-based mesoporous electrodes while keeping their reversible photochromic behavior after integration in complete devices. The resulting smart solar cells can generate electricity and self-adapt themselves depending on the light intensity in order to be more transparent under low light intensity.

In this work, we propose a new strategy for designing spiro-indoline naphthoxazine (SINO) and spiro-indoline naphtho-pyran (NIPS) dyes with the goal to explore their potential for solar cells. These two families of photochromic dyes are well known for their excellent switching kinetics and good resistance to photodegradation.[25] As with diphenyl-naphthopyrans, the mechanism of the photochromic reaction of SINO and NIPS involves the cleavage and reformation of the carbon-oxygen single bond of the oxazine or pyran rings, respectively, as shown in Scheme 1. In the previous work on this type of dyes, the spiro-indoline benzopyran (BIPS) sensitizer carried the carboxylic anchor away from the conjugated system and its SINO counterpart did not even have a suitable anchoring function, leading to extremely poor performances in solar cells.[24] For this reason, we designed two SINO and two NIPS photosensitizers following a donor–π–acceptor (D–π–A) structure (Scheme 1). Then, we investigated their optical and photochromic properties with the goal to establish new structure–properties relationships for this class of molecules. Then we used these molecules as photosensitizers in DSSCs to compare their photovoltaic performances.

2. Design and synthesis

Upon irradiation, SINO and NIPS are known to lead to the formation of merocyanine forms (MC) with a cation localized on the indoline nitrogen after opening the oxazine or pyran ring of their closed forms (CF).[26] Therefore, it seems reasonable that the introduction of the anchoring function must be on the naphthalene part of the molecule to favor the injection into the oxide. To verify this hypothesis and to identify the position on which this function must be introduced, density-functional theory (DFT) calculations have been performed on the SINO reference (Fig. S24, ESI†).[27] Three positions easily accessible by synthesis have been selected for this modeling study, *i.e.* the 8′, 5, and 6′ positions for SINO8′, SINO5 and SINO6′ respectively. From the calculated energies, we noticed that all the molecules have highest/lowest occupied molecular orbitals (HOMO and LUMO respectively) energy levels correctly positioned with respect to the conduction band of the oxide and with respect to the potential of the redox mediator. The HOMO levels are found between −5.3 and −5.7 eV and the LUMO are lying between −2.9 and −3.2 eV with respect to the vacuum level. In other words, the three molecules can sensitize the oxide and be regenerated by the iodine-based electrolyte, both in their initial and isomerized state. The determination of the HOMO and LUMO orbital distributions is more useful. Indeed, the LUMO of the open forms of SINO8' and SINO5 are delocalized on the whole molecule so they will not be suitable for a good injection, while the LUMO of SINO6' is a little more localized on the acceptor part. Therefore, it could potentially lead to a more efficient injection of electrons into the oxide. For this reason, the anchoring functions, either a *p*-phenyl-carboxylic acid or a *p*-phenyl-cyanoacrylic acid, were introduced in the 6′ position. In addition, to reinforce the electron-donating character of the indoline unit, a diphenylamine unit substituted by two octyl chains was introduced in the 5 position.

Therefore, we carried out the synthesis of four derivatives: **SINO-1**, **SINO-2**, **NIPS-1** and **NIPS-2**, whose structures and synthesis are depicted in Schemes 2 and 3. In the case of the SINO dyes, the 4-bromo-1-nitrosonaphthalen-2-ol precursor **1** was obtained from 4-bromonaphthalen-2-ol *via* direct nitrosilation in acid medium[28] and it was directly used in the subsequent step without further purification. In the case of 4-formyl-3-hydroxynaphthalen-1-yl trifluoromethanesulfonate required for the synthesis of the NIPS derivatives, a less straightforward pathway was followed. First, naphthalene-1,3-diol was methylated in position **3** prior to introduce the triflate group in position **1**.[29] The carbonyl group was then introduced in position **4** through a Rieche formylation and eventually the alcohol was deprotected in the presence of boron tribromide to obtain the naphthol **5**. On the other hand, to prepare the donating block **6**, the Fischer's base was first brominated according to previously reported conditions[30] and then the diphenylamine moiety was introduced through a Buchwald-Hartwig amination.

The condensations between the Fischer's bases and the naphthol derivatives were carried out in ethanol or toluene for the NIPS and SINO derivatives respectively to obtain intermediates **7–10** (Scheme 3). Finally, and in view of the lack of stability of the photochromes in the conditions used in the Knoevenagel condensations, the anchoring functions were directly introduced in the Suzuki coupling together with the phenyl spacer, for either the benzoic or the 2-cyano-3-phenylacrylic acceptors. This procedure, which is a deviation from the conventional synthetic way of introducing the anchoring functions, allowed obtaining the target molecules in a straightforward manner with overall yields between 5% and 18%.
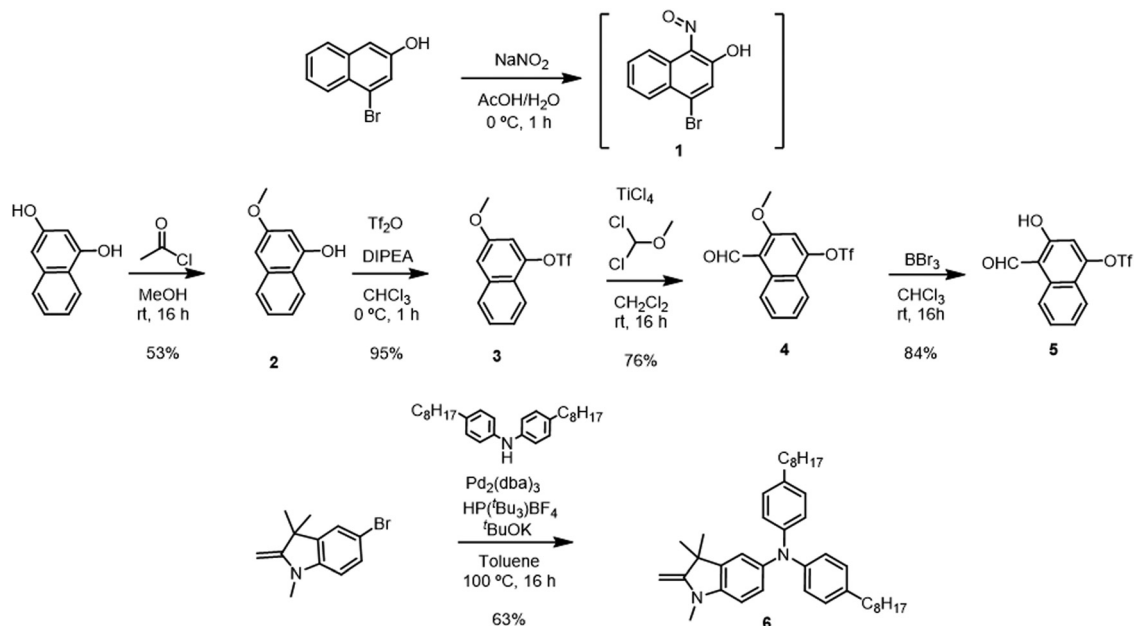
Scheme 2 Synthetic pathway followed to obtain precursors **1**, **5** and **6**. DIPEA: *N,N*-diisopropylethylamine; Tf: trifluoromethylsulfonyl, dba: benzylideneacetone.
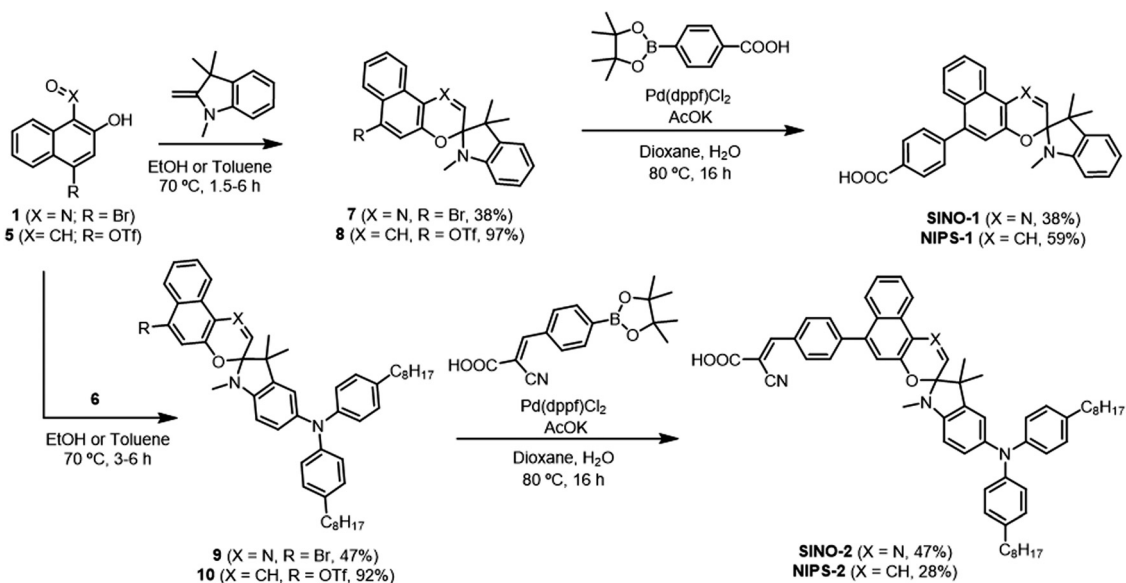
Scheme 3 Synthetic pathway used to obtain the new dyes **SINO-1**, **SINO-2**, **NIPS-1** and **NIPS-2**. dppf: (diphenylphosphino)ferrocene.

3. Optical properties under different stimuli

3.1. Photochromic properties

Despite the large number of studies devoted to SINO and NIPS molecules, structure–photochromic property relationships are only available for a restricted number of compounds and only few reports are dealing with push–pull effects within these families.[31] Since toluene, tetrahydrofuran (THF) and dimethylformamide (DMF) are commonly used solvents to characterize

the photochromic behavior of photochromic dyes, we decided to use them in this study (Fig. S25–S27, ESI,† and Table 1). As an example, we show the spectra obtained in DMF in Fig. 1. In every solvent, the absorption patterns of the colorless forms exhibit localized π–π* transitions in the UV range, corresponding to the two orthogonal halves of each molecule.[32]

In good agreement with different examples in the literature, both SINO derivatives exhibit a photochromic behavior upon irradiation. In these conditions, the ICT band of the open-form isomers emerges above 600 nm, slightly redshifted in the case

Table 1 Optical properties of the four new compounds in 2 × 10^{-5} M solutions in toluene, THF and DMF at 25 °C. The MC forms were generated by irradiation with a 200–600 nm/200 W xenon lamp and the MCH forms by addition of HCl

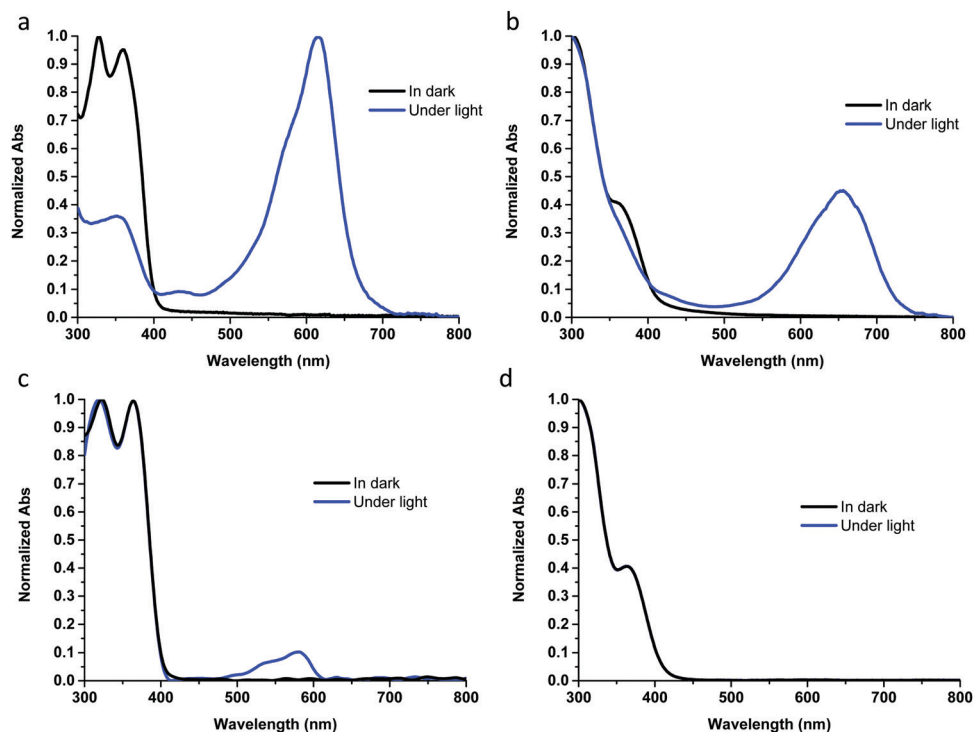| Dye	$\lambda_{\text{max Tol}}$ CF (nm)	$\lambda_{\text{max Tol}}$ MC (nm)	$\lambda_{\text{max Tol}}$ MCH (nm)	$\lambda_{\text{max THF}}$ CF (nm)	$\lambda_{\text{max THF}}$ MC (nm)	$\lambda_{\text{max THF}}$ MCH (nm)	$\lambda_{\text{max DMF}}$ CF (nm)	$\lambda_{\text{max DMF}}$ MC (nm)	$\lambda_{\text{max DMF}}$ MCH (nm)
SINO-1	329	605	556	329	608	593	328	615	541
SINO-2	310	652	604	305	658	601	302	654	585
NIPS-1	367	569	499	325	—	512	325	579	488
NIPS-2	306	—	582	304	—	563	300	—	555

Fig. 1 UV-vis absorption spectra of (a) **SINO-1**, (b) **SINO-2**, (c) **NIPS-1** and (d) **NIPS-2** in 2 × 10^{-5} M DMF solutions at 25 °C in the dark and under light using a 200–600 nm/200 W xenon lamp.

of **SINO-2**. This effect is consistent with the higher push–pull effect induced by the two substituents. Compared to SINO compounds, their NIPS counterparts exhibited a limited photochromic behavior, a phenomenon that has been already reported for this type of derivatives.[33] However, a slight band at *ca.* 570 nm could be observed under illumination in the case of **NIPS-1**, in both toluene and DMF, but surprisingly this compound was not photochromic when studied in THF. To the contrary, **NIPS-2** does not show photochromic properties in any of the solvents. For **SINO-1**, **SINO-2** and **NIPS-1**, it is noteworthy that the maxima of the absorption bands do not change much from one solvent to the other for either the CF or MC forms. It is also important to note that the three photochromic dyes can be colored with exposure to polychromatic light, an important aspect for the targeted application. Then, we investigated the thermal discoloration kinetics of the new compounds. Once the photostationary state (PSS) was reached under illumination (after *circa* 60 s), the irradiation source was turned off and the obtained discoloration curves were then modelled through the

following equations with single and double exponentials respectively depending on the obtained experimental results:

$$A(t) = a_1 e^{-k_1 t} + A_\infty; \quad A(t) = a_1 e^{-k_1 t} + a_2 e^{-k_2 t} + A_\infty$$

where, $A(t)$ is the absorbance of the solution, k_n is the thermal discoloration kinetic constant (in s^{-1}), an is the amplitude of the kinetics of this process, and A_∞ is the residual absorbance.

The photochromic SINO derivatives showed extremely fast bleaching kinetics and the discoloration was even faster for **NIPS-1**. In all cases, no persistent colored isomers are formed after exposure to light (Table 2, Fig. 2 and Fig. S28, ESI†) and the solutions are fully decolored in less than 10 s for the SINO dyes and less than 1 s for the photochromic NIPS dye. However, they are more than 100 times faster compared to those of the best performing naphthopyran photochromic dyes in DSSCs, which make these molecules particularly appealing for application in semitransparent solar cells with dynamic optical properties. These values are in good accordance with the ones reported for unsubstituted SINO and NIPS.[25] It is also noticeable that in

Table 2 Kinetic discoloration constants of **SINO-1**, **SINO-2** and **NIPS-1** in 2×10^{-5} M solutions in toluene, THF and DMF at 25 °C from their MC form. *k_2 constant of the bi-exponential decay

| Dye	k (s^{-1}) Toluene	k (s^{-1}) THF	k (s^{-1}) DMF
SINO-1	0.59	1.2	0.77
SINO-2	0.58; 3.8×10^{-2}*	0.83	0.51
NIPS-1	28	—	8.1
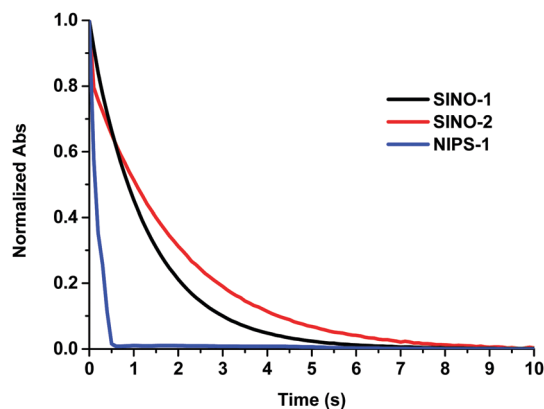
Fig. 2 Normalized discoloration curves of **SINO-1**, **SINO-2** and **NIPS-1**, example given in DMF in 2×10^{-5} M solutions at 25 °C in the dark after irradiation 60 s with a 200–600 nm/200 W xenon lamp.

every case a mono-exponential decay was obtained except for **SINO-2**, which exhibits the slowest kinetics and a bi-exponential decay in toluene likely due to the formation of different isomers.

3.2. Acidochromic properties in the dark

The compounds synthesized in this study are designed to be integrated in a DSSC device configuration with a liquid electrolyte, which usually contains many additives, I$_3^-$/I$^-$ couple as redox mediator and electrolytes often show a pH below 7. However, it is well known that SINO and NIPS are acid-sensitive and they usually possess acidochromic properties.[34–36] According to the literature, this type of derivatives are rapidly converted into their respective protonated open forms (MCH) in the presence of strong acids in an *E* conformation (Scheme 4). This is why it seemed important to address this aspect.

We found that the four new derivatives revealed acidochromic properties in absence of light. In order to study the interaction between protons and our new SINO and NIPS molecules, a titration with HCl was carried out in THF in the dark (Fig. 3).
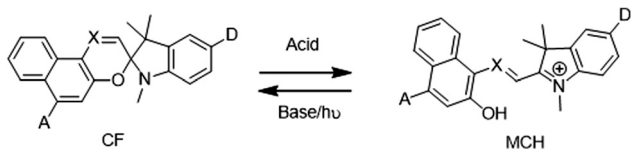
Scheme 4 Interconversion between the close (CF) and open protonated forms (MCH) of SINO (X = N) and NIPS (X = CH) derivatives in the presence of strong acids.

It can be observed that the increase in the absorption of the band related to the MCH form when HCl is added. In addition, a sole isosbestic point was monitored in every case, suggesting that the protonation gives rise to a single compound, namely the MCH form.[37,38] It appears from the spectra presented in Fig. 3 that the SINO compounds are less sensitive to acidic conditions compared to their NIPS analogs, as only a small fraction of the molecules undergoes the protonation reaction. For **SINO-1**, **SINO-2** and **NIPS-1**, the absorption band of the MCH form in the visible is blue-shifted compared to the MC. The shifts varied between 15 and 70 nm for the SINO derivatives and from 70 to 90 nm for **NIPS-1** depending on the solvent. In contrast to the CF and MC forms, the maxima of the bands associated with the MCH form are shifted depending on the solvent used due to its charged nature,[39] although it does not follow a specific trend. This indicates that only MCH are subjected to solvatochromism. In addition, the acidochromism was found to greatly depend on the strength of the acid used. This observation confirms the results reported for the BIPS family.[40] The acidochromic effect is observed when strong acids that can protonate the MC form are used. For instance, in the case of **NIPS-1**, the colored form was observed when acids with pK_a below 0.5 were employed (*i.e.* nitric, sulfuric, hydrochloric and perchloric acids) but not in the case of "weaker" acids (*i.e.* trifluoroacetic, phosphoric or acetic acids) (Fig. S29, ESI†). Our experiments show that the nature of the acid plays a critical role on the protonation and the formation of the MCH. Further experiments are required to elucidate the exact role of the counter ions on the acidochromic properties of these dyes.

3.3. Acidochromic properties under illumination

Under the conditions of use that we envisaged for these compounds in solar cells, the dyes will not only be exposed to a low pH environment but also to light. This is why it seemed interesting to investigate their photochromic and acidochromic behaviors by combining the two stimuli. Therefore, the compounds in their protonated form in solution were therefore exposed to light. First, it should be noted that the SINO derivatives still exhibited a positive photochromism, *i.e.* a coloration upon irradiation, but the discoloration kinetic constants were found to be lower in the presence of acid (Fig. S30, ESI†). This could be explained by the fact that a large proportion of these compounds still exists in closed form even in the presence of acid as suggested by the weak intensity of the band corresponding to MCH in Fig. 3.

More interestingly, in stark contrast to the SINO compounds, the MCH forms of the NIPS exhibit a negative photochromic behavior.[41] According to the literature of spiro-indoline benzopyrans, this process implies an *E–Z* isomerization followed by the deprotonation and the consequent ring closure.[42]

Although the effect is not intense in the case of **NIPS-2**, **NIPS-1** reverts to its initial state under illumination and it is able to reopen quite rapidly in the dark (with a k of *circa* 2.6×10^{-2} s^{-1}) (Fig. 4). The high reversibility of this process in THF has to be highlighted, as **NIPS-1** bleaches almost quantitatively under
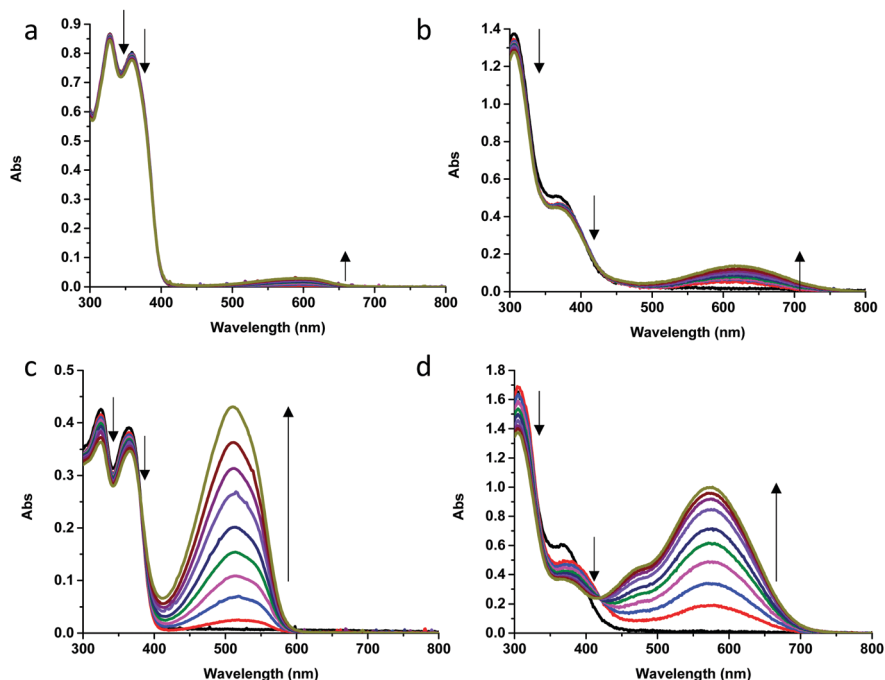
Fig. 3 Absorption titration of (a) **SINO-1**, (c) **NIPS-1** (5×10^{-5} M), (b) **SINO-2** and (d) **NIPS-2** (2.5×10^{-5} M) with increments of 70 and 140 eq. of HCl respectively in THF solutions in the dark at 25 °C.

illumination even reaching the same level of coloration in the dark showing no sign of photodegradation. Though this effect has been observed in the case of some spiro-indoline benzopyran derivatives,[43] to the best of our knowledge, it has not been reported for NIPS compounds. It should also be noted that this negative photochromism observed in solution when acidic conditions and light are combined could be modulated by changing the solvent and the nature of the acid (see Fig. 4).

To conclude this section, it seems that the molecules once incorporated in a device in the presence of a liquid electrolyte, will be able to exist in multiple forms: either in a closed form, an open form of MC type but also in an open MCH form after protonation. For this reason, it is important to verify if the different possible forms of these molecules present energy levels appropriately positioned for an efficient sensitization of the oxide and an efficient regeneration by the redox mediator that we have chosen, namely the I_3^-/I^- couple.[44] The energy levels of the dyes are discussed in the next section.

4. Energy levels and theoretical calculations

With the goal to unravel how the optoelectronic properties of the dyes change by swapping from the closed to the opened forms, and how the substitution and the nature of the photochromic unit influence the energy levels of the frontier orbitals, we performed cyclic voltammetry experiments in dichloromethane in the dark (Fig. S31, ESI†). Contrarily to diphenyl-naphthopyran dyes,[20] the open-form isomers of SINO and NIPS

compounds cannot be accumulated in sufficient amount in solution to allow the determination of the HOMO and LUMO energy levels for these isomers, so only the HOMO of the CF could be experimentally characterized. Therefore, the energy levels of the frontier orbitals of the opened forms were evaluated by ground-state density-functional theory calculations at the B3LYP/TZ2P level of theory (Fig. 5 and ESI† for details). However, it should be taken into account that the electronic landscape of the dyes in real device configuration may vary. First, the HOMO energies obtained for the CF by means of theoretical calculations are in good accordance with the one obtained by cyclic voltammetry (all comprised between -4.9 eV and -5.6 eV), thus validating the theoretical approach. Then, when we compare equivalent forms for each dye, the theoretical trend is the same within the **NIPS-1**/**SINO-1** and **NIPS-2**/**SINO-2** pairs. The results indicate that the delocalisation of the orbitals on the backbone of the molecule and the energy levels positions are mostly influenced by the modification of the electron-donor and electron-acceptor groups, and not by the nature of the photochromic unit. First, we observe that for all the compounds the band gap is reduced going from the close to the open forms, being the levels of the MCH forms substantially downshifted. As for diphenyl naphthopyran dyes, the LUMO energy levels of the open-form isomers are shifted towards more negative values. This leads, in the case of SINO derivatives, to LUMO energy levels of MCH close to the one of the TiO_2 conducting band, which could end up in a reduced driving force for the photo-induced injection of electrons from the excited state of the dyes. For the NIPS family, the shift of the LUMO energy levels for the MCH forms is less problematic
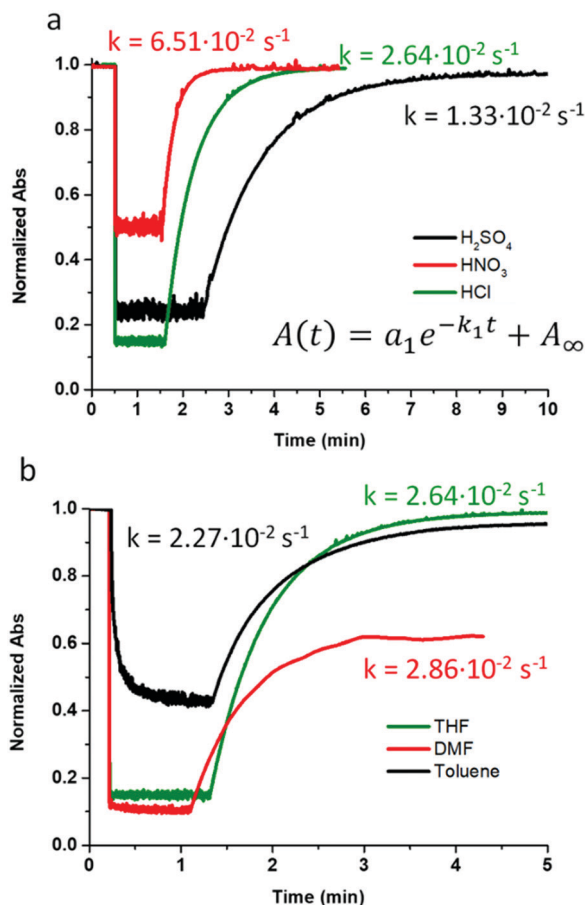
Fig. 4 Coloration kinetics of **NIPS-1** (2×10^{-5} M in the dark at 25 °C after illuminating with a 200–600 nm/200 W xenon lamp) (a) after the addition of 1 drop of different acids in THF and (b) in THF, DMF and toluene after the addition of 1 drop of HCl.

$$A(t) = a_1 e^{-k_1 t} + A_\infty$$

since a driving force of *circa* 0.3 eV is conserved. Comparing **SINO-1** to **SINO-2** and **NIPS-1** to **NIPS-2**, it appears that the stronger electron withdrawing character of the cyano-acrylic acid function shifts the LUMO energy levels downward except for the MCH forms. It is also clear that the introduction of a diphenylamine donor group on the indoline part has a strong impact on the HOMO level of the molecules that are shifted towards more positive values.

Apart from the energy levels, the spatial distribution of the frontier orbitals is also a critical parameter because the efficiency of the injection and regeneration processes will strongly depend on it. Even though in all the CF the HOMO is localized on the donor and the LUMO on the acceptor showing a suitable electron distribution along the molecules, it is not the case for all the open forms. In the case of **NIPS-1** and **SINO-1**, the HOMO and LUMO distributions of either the MC or MCH lie basically in the same region, *i.e.* the photochromic core, thus probably hampering the injection of electrons into the conduction band of the TiO_2 electrode. However, though for the MC form of **NIPS-2** and **SINO-2** there is clearly a suitable spatial distribution between the donor and the acceptor for a charge transfer effect, we observe again the LUMO contribution in the

central part of the molecule for their MCH forms, which may hinder the electron injection as well.

5. Photovoltaic properties

The photovoltaic performances of the SINO and NIPS dyes were evaluated in opaque DSSC configurations. We recorded current–voltage characteristics in the dark and at different time intervals of exposure to light, and the short-circuit current density (J_{sc}), open-circuit voltage (V_{oc}), fill factor (FF) and PCE were determined. Two types of electrolyte were employed for the fabrication of the solar cells, a homemade electrolyte[20] that was specifically designed for photochromic naphthopyran dyes, and a commercial one known as Iodolyte (Solaronix). The main difference of our electrolyte in comparison to the latter is a 3-fold increase in I_2 and the lack of some additives, such as guanidinium thiocyanate and *tert*-butylpyridine, thus modifying the final pH. The results are reported in Fig. 6 and Table 3. The TiO_2 mesoporous electrodes were sensitized with the dyes in the presence of chenodeoxycholic acid (CDCA) to avoid aggregation (see ESI† for details). It should be noted that during this step a very light coloration of the dyes occurs on the surface of the electrode (Fig. S32 and S33, ESI†). This faint coloration is attributed to the formation of MCH due to residual traces of acid in the pores of TiO_2 after the $TiCl_4$ treatment. The huge different proton affinity between NIPS and SINO observed in solution is less appreciable once the molecules are grafted onto the semiconductor. Then, after sealing the electrodes, the electrolyte was introduced in the devices. Note that when our homemade electrolyte is introduced and reaches the electrode, all four dyes switch instantaneously to the open MCH form and appear to be locked in this conformation (Fig. S33, ESI†). This coloration is a clear manifestation of the acidochromic behavior of the dyes and the stabilization of the MCH form due to the acidic pH of this electrolyte. Indeed, we could determine a pH between 1 and 2 for this electrolyte. This acidochromic phenomenon, which consequently induces the loss of photochromic behavior, has not been reported in previous reports on spiropyran and spiroxazine-based DSSCs, even though a comparable iodine-based redox mediator was used.[24] On the contrary to what was observed in solution, the negative photochromism of NIPS derivatives was not observed once the dyes were grafted on the electrodes and embedded in the devices. This is confirmed by the absence of decrease in J_{sc} after several successive J–V measurements. Even though, the current density for all dyes appears limited with this electrolyte (< 3.5 mA cm^{-2}).

Referring to theoretical calculations in previous section, in the SINO series the formation of the MCH strongly decreases the ability to inject electrons into the conduction band of TiO_2. Indeed, the LUMO level is lowered, thus reducing the driving force, and its spatial localization is quite far from the anchor group, not allowing a correct sensitization of the TiO_2. This explains the poorer performance of SINO compared to their NIPS counterparts. The same problems appear with the NIPS
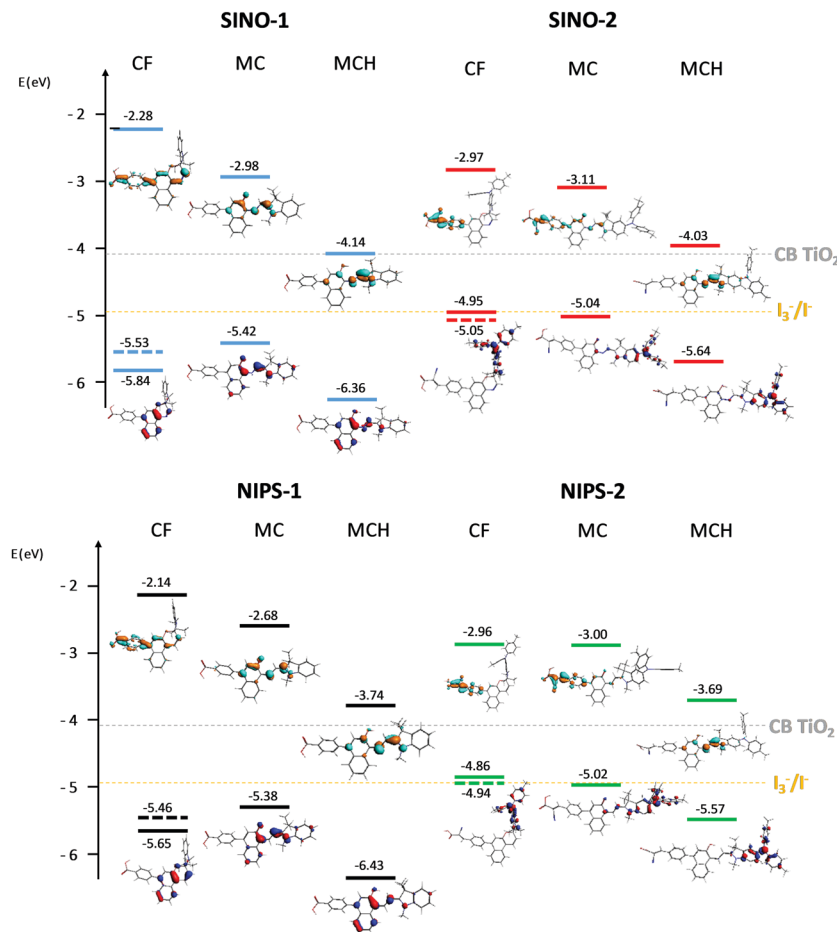
Fig. 5   DFT-calculated energy levels (*versus* the vacuum level) of the frontier orbitals of the four new dyes and their spatial localizations in closed (CF), merocyanine (MC) and protonated merocyanine forms (MCH) (full lines). Experimental values of the CF obtained by CV are shown in dashed lines. The potential of the I_3^-/I^- pair (*ca.* −4.95 eV) and the TiO_2 conduction band (*ca.* −4.10 eV) are shown in yellow and grey dashed lines respectively.

compounds, but in that case, the LUMO energy level of the MCH is higher giving rise to a slightly higher driving force towards the injection. In contrast, when the commercial Iodolyte was used, the level of staining was considerably lower (Fig. 6). This is explained by its pH around 7, which allows the closed form to be present in the absence of illumination. In this case, the photochromic behavior is preserved for the molecules that were already demonstrated photochromic in solution, *i.e.* the two SINO derivatives and **NIPS-1**. In addition, Iodolyte contains additives such as *tert*-butylpyridine that is known to shift the TiO_2 conduction band upwards thus increasing the V_{oc}. However, in spite of all that, the overall performances of the three photochromes remain in the same range. According to theoretical calculations, the spatial distribution of the LUMO that delocalizes to the core of the molecule on the MC forms may explain this result for **SINO-1** and **NIPS-1**. Surprisingly, in the case of **NIPS-2**, despite its lack of photochromic behavior and thus an absence of open MC form absorbing in the visible, a better current density was recorded contrarily to the other sensitizers. **NIPS-2** demonstrates a J_{sc} higher than 5 mA cm^{-2} and a V_{oc} over 0.6 V, thus leading to the highest PCE ever reported for this family of molecules: 2.73%. In addition, these devices are

relatively stable as they are able to maintain their V_{oc} after *ca.* 5000 h under ISOS-D1 ageing test[45] though the J_{sc} is substantially reduced, resulting in an efficiency loss of 47% (Fig. S34, ESI†).

The lack of coloration of this device may indicate that most of **NIPS-2** stays in its CF. To confirm the contribution of each form in **NIPS-2**/Iodolyte-based devices, the absorption patterns of 2 μm transparent devices made of both electrolytes were recorded (Fig. 7). It is noteworthy that when the homebased electrolyte is used, an intense absorption band appears in the visible corresponding to the formation of MCH, whereas with Iodolyte the device shows the typical yellow color of the Iodine based electrolyte and the absorption spectrum remains flat in the visible. In addition, as it can be observed in the incident photon to current efficiency (IPCE) spectrum of the 13 μm device composed of the homemade electrolyte (Fig. S35, ESI†), in spite of the great coloration, the injection of electrons related to the MCH form is negligible, in good agreement with the results provided by the theoretical calculations. This also demonstrates that the main contributor to the photogeneration is indeed the CF, favored by the good spatial distribution of its LUMO orbital. Then, to understand the electrolyte-driven behavior of the devices presented in Fig. 6 and Table 3,
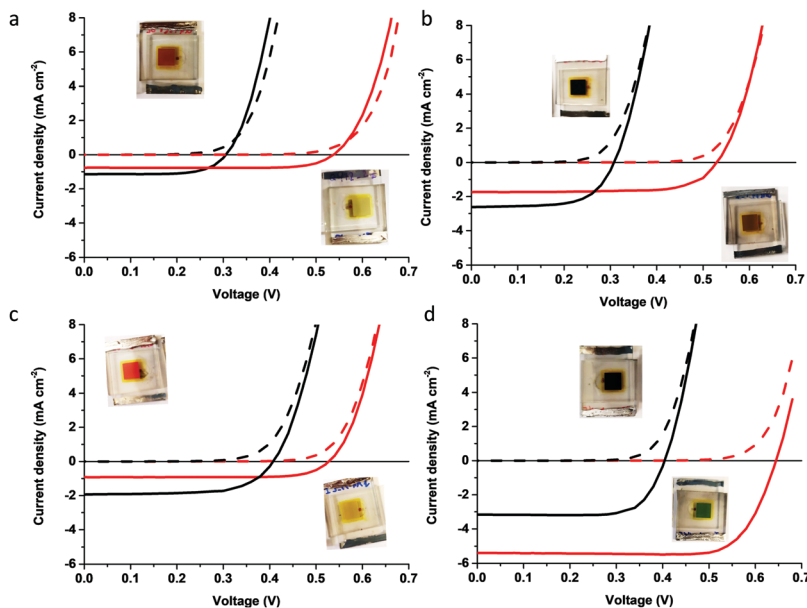
Fig. 6 J–V curves of the 13 μm DSSCs using (a) **SINO-1**, (b) **SINO-2**, (c) **NIPS-1**, and (d) **NIPS-2** as sensitizers under standard irradiation conditions AM 1.5 G, 1000 W m^{-2}; 25 °C (active area = 0.36 cm^2) using our homemade electrolyte (black) and Iodolyte (red) and the pictures of the respective devices in the absence of illumination.

Table 3 Photovoltaic parameters of the DSSCs made of **SINO-1**, **NIPS-1**, **SINO-2** and **NIPS-2** under standard irradiation conditions AM 1.5 G, 1000 W m^{-2}, 25 °C (active area: 0.36 cm^2). Average values in brackets over minimum two cells

Dye	Electrolyte	J_{sc} (mA cm^{-2})	V_{oc} (V)	FF (%)	PCE (%)
SINO-1	Homemade	1.14 (1.09)	0.31 (0.28)	68 (67)	0.24 (0.20)
	Iodolyte	0.76 (0.76)	0.54 (0.54)	79 (78)	0.32 (0.32)
SINO-2	Homemade	2.62 (2.53)	0.31 (0.31)	64 (64)	0.51 (0.50)
	Iodolyte	1.74 (1.70)	0.53 (0.53)	72 (72)	0.66 (0.65)
NIPS-1	Homemade	1.94 (1.76)	0.41 (0.38)	66 (64)	0.52 (0.42)
	Iodolyte	0.92 (0.90)	0.53 (0.52)	77 (75)	0.38 (0.35)
NIPS-2	Homemade	3.16 (3.14)	0.40 (0.40)	74 (74)	0.94 (0.94)
	Iodolyte	5.39 (5.11)	0.64 (0.65)	78 (80)	2.73 (2.62)

Fig. 7 UV-Vis spectra and pictures of the respective devices of **NIPS-2**-based DSSCs on 2 μm transparent TiO$_2$ electrodes using Iodolyte and our homebased electrolyte in the absence of illumination.

an electrochemical impedance investigation was carried out on the DSSCs made of the best performing dye, **NIPS-2**, and both electrolyte compositions. Charge transfer resistances were measured (see Fig. 8).

The main arc of the impedance spectra (see Fig. S36a and b, ESI†) was fit to a single –RC– equivalent circuit element where the resistance is considered the charge transfer resistance (dark) or recombination resistance (R_{CT}) and the capacitance is the chemical capacitance (C_μ). Both parameters are known to show an exponential voltage dependence following eqn (S1), (S2) and (Fig. S36c–f) (ESI†).[46,47] The extracted α and β for the **NIPS-2** DSSC using Iodolyte and the homebased electrolyte at dark conditions and under illumination are collected in Table S1 (ESI†). Typical values for α and β values normally reported for DSSCs are in the range of 0.15–0.35 for α and 0.5–0.8 for β.[48–51] While the α parameter, which shows the average depth of the traps, remained within the range typical for a DSSC configuration irrespective of the redox couple used, β varied depending on the electrolyte.

When Iodolyte was employed, this parameter changed from 0.56 to 0.73 between the irradiation conditions but still within the DSSC typical values. However, when our homebased electrolyte was used in turn, β changed from 0.75 in the dark to 1.04 under operating conditions, which suggests a possible change in the dominant recombination pathway, which normally in DSSCs correspond to triiodide reduction.[52,53] Whatever the redox couple, no TiO$_2$ conducting band shift was induced at irradiation conditions (Fig. S36, ESI†). However, as it can be observed in Fig. S37 (ESI†), the change of the electrolyte induces a bandshift of +226 mV and +220 mV with Iodolyte under dark and white light irradiations, respectively, explaining the higher photovoltage observed in the reported JV curves.
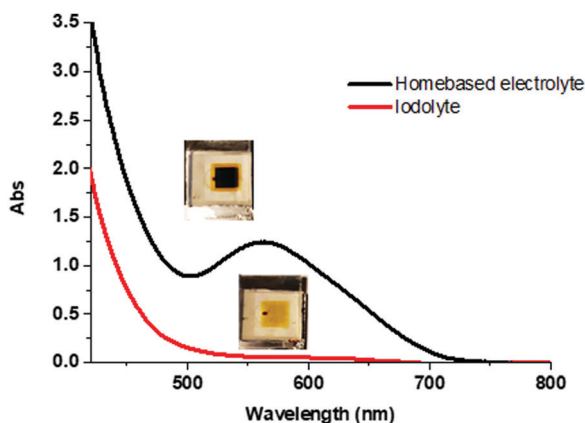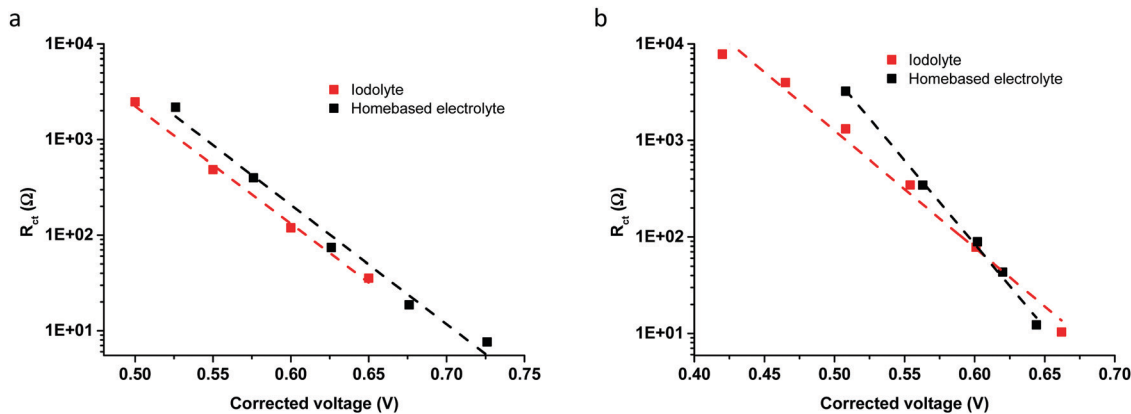
Fig. 8 Charge transfer resistances comparisons at the same quasi-Fermi level of 13 μm DSSCs made of **NIPS-2** and both electrolytes (a) in the dark and (b) under operating conditions.

The Nyquists plots under irradiation, in which the size of the real part of the recombination arc is approximately equal to the recombination resistance, were compared applying a voltage correction to account for the bandshift, ensuring that both measurements were done at a similar electron concentration at the quasi-Fermi level (Fig. S38, ESI†). The diameter is larger in homebased electrolyte-based cells despite the high I_2 concentration and the lower V_{oc} therein. Certainly, the acidic home-made electrolyte gives rise to the protonated merocyanine form facilitating the interaction of the positively charged center with I_3^- hence lowering its local concentration at the photoanode

Fig. 9 (a) $J–V$ curve of the 13 μm **NIPS-2**/Iodolyte-based DSSCs under standard irradiation conditions AM 1.5 G, 1000 W m^{-2}; 25 °C (active area = 0.36 cm^2) and (b) respective transmittance spectrum together with a picture of the actual device.

compared to Iodolyte. This can also explain the change observed in the β values compared to the range usually reported for DSSCs.

Eventually, in an attempt to obtain the most performing semi-transparent device with the couple **NIPS-2**/Iodolyte, DSSCs were fabricated using a transparent 13 μm TiO$_2$ anode (Fig. 9). On such thick electrodes, the coloration is more pronounced due to the formation of the MCH form with the remaining traces of acid, thus leading to slightly greenish electrodes. Despite of that, a PCE of 2.18% was then recorded while keeping the AVT at 52%, mostly absorbing below 500 nm, demonstrating once again that the majority of the molecules is in its CF as the transmittance at longer wavelengths is always kept above 50%. This corresponds to a light utilization efficiency (LUE) of 1.13. Then, to determine the aesthetic quality of the semi-transparent devices, the Commission Internationale de l'Eclairage (CIE) color coordinates were determined, as well as the color rendering index (CRI), which revealed an acceptable value of 80.4% (Fig. S39, ESI†).[54,55] Therefore, despite its lack of photochromic behavior, this result shows that this type of dyes can be used in semi-transparent DSSCs. Eventually, though modest, they remain as the best results for SINO and NIPS derivatives in the literature.
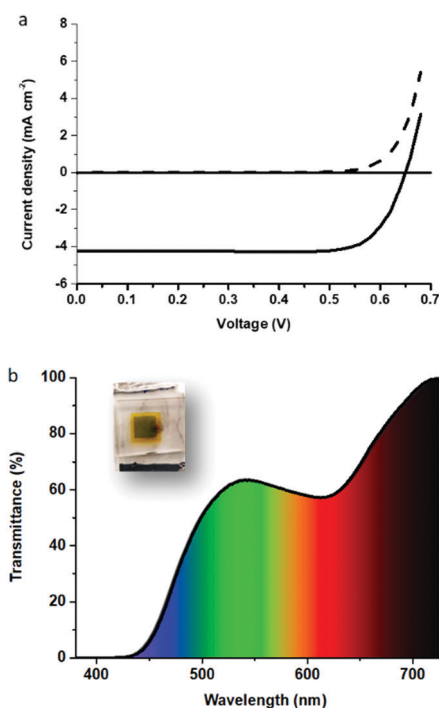
6. Conclusion

In this study, we investigated the potential of two families of photochromic dyes, *i.e.* spiro-indoline naphthopyran and spiro-indoline naphthoxazine for their use in dye-sensitized solar cells. We proposed an original molecular design to obtain photochromic molecules that can sensitize TiO$_2$ and be regenerated by an iodine-based electrolyte. We studied the photochromic and acidochromic behavior of these compounds. We highlight a positive photochromism in solution for only three of the compounds, photochromism which is characterized by extremely fast thermal discoloration kinetics. On the other hand, all the compounds have an acidochromic behavior and lead to the formation of protonated merocyanines absorbing in the visible range under acidic conditions. When the compounds

are studied in acidic conditions under illumination, they show different behaviors. The spiro-indoline naphthoxazines keep a positive photochromism while the spiro-indoline naphthopyrans show a negative photochromism.

These studies allow us to rationalize the behavior of these molecules when they are incorporated in solar cells. We demonstrate that the choice of the electrolyte is crucial as it drives the optical behavior of these compounds. The use of an acidic electrolyte suppresses the photochromic behavior in device whereas with a neutral pH electrolyte, the photochromic behavior is preserved. Although the photochromic behavior is not preserved in all devices with these dyes, these results show that they can be used in DSSCs. The results remain modest with a maximum PCE of 2.7%, but they are significantly improved compared to previous reports on spiropyran and spiroxazine derivatives in the literature. Eventually, the best performing dye, **NIPS-2**, despite its lack of photochromism, allowed obtaining a PCE of 2.7% in opaque solar cells and 2.2% in semi-transparent ones while showing an AVT at 52%.

This study is the first to investigate in details the complex relationships between photochromic, acidochromic and photovoltaic properties for these two families of dyes. The structure–property relationships that we establish in this study will undoubtedly be useful for the development of new photochromic compounds with optimized optoelectronic properties for applications in various fields, including photovoltaics.

Author contributions

Q. H., J. L. and J. M. A. C. synthesized and characterized the dyes. P. M. and J. M. A. C. performed the DFT calculations. V. M. M., and J. M. A. C. fabricated and characterized the solar cells and V.M.M performed the EIS measurements and analyzed the data with J. A. A. A. J. R. performed the IPCE measurements. R. D. designed the materials and experiments. R. D. and J. M. A. C. treated the data and wrote the manuscript, with contributions from all authors. All authors have given approval to the final version of the manuscript.

Conflicts of interest

There are no conflicts to declare.

Acknowledgements

Notes and references

1 J. Zhang, J. Wang and H. Tian, *Mater. Horiz.*, 2014, **1**, 169–184.
2 R. Pardo, M. Zayat and D. Levy, *Chem. Soc. Rev.*, 2011, **40**, 672.
3 S. Jia, W.-K. Fong, B. Graham and B. J. Boyd, *Chem. Mater.*, 2018, **30**, 2873–2887.
4 S. Brazevic, S. Nizinski, R. Szabla, M. F. Rode and G. Burdzinski, *Phys. Chem. Chem. Phys.*, 2019, **21**, 11861–11870.
5 L. Kortekaas and W. R. Browne, *Chem. Soc. Rev.*, 2019, **48**, 3406–3424.
6 V. Malatesta, C. Neri, M. L. Wis, L. Montanari and R. Millini, *J. Am. Chem. Soc.*, 1997, **119**, 3451–3455.
7 S.-Z. Pu, Q. Sun, C.-B. Fan, R.-J. Wang and G. Liu, *J. Mater. Chem. C*, 2016, **4**, 3075–3093.
8 M. Dong, A. Babalhavaeji, S. Samanta, A. A. Beharry and G. A. Woolley, *Acc. Chem. Res.*, 2015, **48**, 2662–2670.
9 S. Nigel Corns, S. M. Partington and A. D. Towns, *Color. Technol.*, 2009, **125**, 249–261.
10 G. Berkovic, V. Krongauz and V. Weiss, *Chem. Rev.*, 2000, **100**, 1741–1754.
11 M. Irie, T. Fukaminato, K. Matsuda and S. Kobatake, *Chem. Rev.*, 2014, **114**, 12174–12277.
12 M. Qin, Y. Huang, F. Li and Y. Song, *J. Mater. Chem. C*, 2015, **3**, 9265–9275.
13 W. Szymański, J. M. Beierle, H. A. V. Kistemaker, W. A. Velema and B. L. Feringa, *Chem. Rev.*, 2013, **113**, 6114–6178.
14 R. A. Evans, T. L. Hanley, M. A. Skidmore, T. P. Davis, G. K. Such, L. H. Yee, G. E. Ball and D. A. Lewis, *Nat. Mater.*, 2005, **4**, 249–253.
15 N. Ishii, T. Kato and J. Abe, *Sci. Rep.*, 2012, **2**, 819.
16 H. J. Kang, K.-I. Joo, Y. Y. Kang, J. Lee, Y. Lee, I. Jeon, T.-H. Lee, W.-G. Koh, J.-H. Choi, H.-R. Kim and J.-W. Ka, *Polym. J.*, 2021, **53**, 539–547.
17 D. Kim, K. Jeong, J. E. Kwon, H. Park, S. Lee, S. Kim and S. Y. Park, *Nat. Commun.*, 2019, **10**, 3089.
18 Y. Xiong, A. Vargas Jentzsch, J. W. M. Osterrieth, E. Sezgin, I. V. Sazanovich, K. Reglinski, S. Galiani, A. W. Parker, C. Eggeling and H. L. Anderson, *Chem. Sci.*, 2018, **9**, 3029–3040.
19 B. W. H. Saes, M. M. Wienk and R. A. J. Janssen, *RSC Adv.*, 2020, **10**, 30176–30185.
20 Q. Huaulmé, V. M. Mwalukuku, D. Joly, J. Liotier, Y. Kervella, P. Maldivi, S. Narbey, F. Oswald, A. J. Riquelme, J. A. Anta and R. Demadrille, *Nat. Energy*, 2020, **5**, 468–477.
21 D. Joly, L. Pellejà, S. Narbey, F. Oswald, T. Meyer, Y. Kervella, P. Maldivi, J. N. Clifford, E. Palomares and R. Demadrille, *Energy Environ. Sci.*, 2015, **8**, 2010–2018.

22 A. Fakharuddin, R. Jose, T. M. Brown, F. Fabregat-Santiago and J. Bisquert, *Energy Environ. Sci.*, 2014, **7**, 3952–3981.

23 W. Wu, J. Wang, Z. Zheng, Y. Hu, J. Jin, Q. Zhang and J. Hua, *Sci. Rep.*, 2015, **5**, 8592.

24 N. M. Johnson, Y. Y. Smolin, C. Shindler, D. Hagaman, M. Soroush, K. K. S. Lau and H.-F. Ji, *AIMS Mater. Sci.*, 2015, **2**, 503–509.

25 C. Salemi-Delvaux, E. Pottier, R. Guglielmetti, R. Dubest and J. Aubard, *Dyes Pigm.*, 1999, **40**, 157–162.

26 F. Wilkinson, D. R. Worrall, J. Hobley, L. Jansen, S. L. Williams, A. J. Langley and P. Matousek, *J. Chem. Soc., Faraday Trans.*, 1996, **92**, 1331.

27 G. te Velde, F. M. Bickelhaupt, E. J. Baerends, C. Fonseca Guerra, S. J. A. van Gisbergen, J. G. Snijders and T. Ziegler, *J. Comput. Chem.*, 2001, **22**, 931–967.

28 S. M. Partington and A. D. Towns, *Dyes Pigm.*, 2014, **104**, 123–130.

29 O. D. C. C. de Azevedo, P. I. P. Elliott, C. D. Gabbutt, B. M. Heron, K. J. Lord and C. Pullen, *J. Org. Chem.*, 2020, **85**, 10772–10796.

30 D. Gale, J. Lin and J. Wilshire, *Aust. J. Chem.*, 1977, **30**, 689.

31 A. V. Metelitsa, V. Lokshin, J. C. Micheau, A. Samat, R. Guglielmetti and V. I. Minkin, *Phys. Chem. Chem. Phys.*, 2002, **4**, 4340–4345.

32 S. Minkovska, B. Jeliazkova, E. Borisova, L. Avramov and T. Deligeorgiev, *J. Photochem. Photobiol., A*, 2004, **163**, 121–126.

33 E. I. Balmond, B. K. Tautges, A. L. Faulkner, V. W. Or, B. M. Hodur, J. T. Shaw and A. Y. Louie, *J. Org. Chem.*, 2016, **81**, 8744–8758.

34 C. D. Gabbutt, J. D. Hepworth and B. M. Heron, *Dyes Pigm.*, 1999, **42**, 35–43.

35 C. D. Gabbutt, J. D. Hepworth, B. M. Heron and S. M. Partington, *Mol. Cryst. Liq. Cryst. Sci. Technol., Sect. A*, 2000, **345**, 323–328.

36 L. Yongchao, Y. Ming, M. Fan, X. Sun and E. T. Knobbe, *Sci. China, Ser. B: Chem.*, 1997, **40**, 535–540.

37 J. Vallet, J.-C. Micheau and C. Coudret, *Dyes Pigm.*, 2016, **125**, 179–184.

38 L. S. Koltsova, N. L. Zaichenko, A. I. Shiyonok and V. S. Marevtsev, *Russ. Chem. Bull., Int. Ed.*, 2001, **50**, 1214–1217.

39 E. B. Gaeva, V. Pimienta, S. Delbaere, A. V. Metelitsa, N. A. Voloshin, V. I. Minkin, G. Vermeersch and J. C. Micheau, *J. Photochem. Photobiol., A*, 2007, **191**, 114–121.

40 C. Roxburgh, *Dyes Pigm.*, 1995, **27**, 63–69.

41 S. Aiken, R. J. L. Edgar, C. D. Gabbutt, B. M. Heron and P. A. Hobson, *Dyes Pigm.*, 2018, **149**, 92–121.

42 H. Chen and Y. Liao, *J. Photochem. Photobiol., A*, 2015, **300**, 22–26.

43 A. D. Pugachev, I. V. Ozhogin, N. I. Makarova, I. A. Rostovtseva, M. B. Lukyanova, A. S. Kozlenko, G. S. Borodkin, V. V. Tkachev, I. M. El-Sewify, I. V. Dorogan, A. V. Metelitsa, S. M. Aldoshin and B. S. Lukyanov, *Dyes Pigm.*, 2022, **199**, 110043.

44 A. Hagfeldt, G. Boschloo, L. Sun, L. Kloo and H. Pettersson, *Chem. Rev.*, 2010, **110**, 6595–6663.

45 R. Roesch, T. Faber, E. von Hauff, T. M. Brown, M. Lira-Cantu and H. Hoppe, *Adv. Energy Mater.*, 2015, **5**, 1501407.

46 J. A. Anta, J. Idígoras, E. Guillén, J. Villanueva-Cab, H. J. Mandujano-Ramírez, G. Oskam, L. Pellejà and E. Palomares, *Phys. Chem. Chem. Phys.*, 2012, **14**, 10285.

47 J. Idígoras, L. Pellejà, E. Palomares and J. A. Anta, *J. Phys. Chem. C*, 2014, **118**, 3878–3889.

48 E. Guillén, L. M. Peter and J. A. Anta, *J. Phys. Chem. C*, 2011, **115**, 22622–22632.

49 J. Bisquert, A. Zaban and P. Salvador, *J. Phys. Chem. B*, 2002, **106**, 8774–8782.

50 J. Bisquert, *Phys. Chem. Chem. Phys.*, 2003, **5**, 5360–5364.

51 J. Bisquert and I. Mora-Seró, *J. Phys. Chem. Lett.*, 2010, **1**, 450–456.

52 Q. Wang, S. Ito, M. Grätzel, F. Fabregat-Santiago, I. Mora-Seró, J. Bisquert, T. Bessho and H. Imai, *J. Phys. Chem. B*, 2006, **110**, 25210–25221.

53 Q. Wang, J.-E. Moser and M. Grätzel, *J. Phys. Chem. B*, 2005, **109**, 14945–14953.

54 C. Yang, D. Liu, M. Bates, M. C. Barr and R. R. Lunt, *Joule*, 2019, **3**, 1803–1809.

55 M. Thomas, M. Michael, P. Michael, S. Nick, W. Kevin, C. Sean, V. Jean, D. Canavan, L. Crowson, K. Lev, O. Leinweber, K. Sharma, S. Sobotka, T. James, M. Dominik, P. Matt, R. Chinmay, E. Pavithra, M. John, P. Ben, L. Manuel, N. Olli, S. Marek, S. Maximilian, H. Sianyi, W. Mike, J. Nishant, W. Omar, R. Pawel, G. Joseph, H. Stephen, S. Jedediah, S. Frederic, S. Geetansh, C. Saransh, S. Ilia, G. Tim, P. Gajendra, T. Nicolas and P. Aurélien, *Colour 0.4.1, Zenodo*, 2022.